Journal of Microscopy

Journal of Microscopy, Vol. 00, Issue 0 2017, pp. 1–10 doi: 10.1111/jmi.12589
Received 7 March 2017; accepted 3 May 2017

The elusive ettringite under the high-vacuum SEM – a reflection based on natural samples, the use of Monte Carlo modelling of EDS analyses and an extension to the ettringite group minerals

VINCENT THIÉRY*,†, VINCENT TRINCAL*,† & CATHERINE A. DAVY‡
*IMT Lille-Douai, Institut Mines Télécom, Department of Civil & Environmental Engineering, LGCgE
†Université de Lille
‡LML FRE CNRS 3723 and L2MGC EA 4114 and Ecole Centrale de Lille, 59651 Villeneuve d'Ascq Cedex, France

Key words. EDS analysis, ettringite, ettringite group minerals, Monte Carlo simulation.

Summary

Ettringite, $Ca_6Al_2(SO_4)_3(OH)_{12}.26H_2O$, or $C_6A\bar{S}_3H_{32}$ as it is known in cement chemistry notation, is a major phase of interest in cement science as an hydration product and in polluted soil treatment since its structure can accommodate with many hazardous cations. Beyond those anthropogenic features, ettringite is first of all a naturally occurring mineral (although rare). An example of its behaviour under the scanning electron microscope and during energy dispersive spectroscopy (EDS) qualitative analysis is presented, based on the study of natural ettringite crystals from the N'Chwaning mine in South Africa. Monte Carlo modelling of the electron-matter interaction zone at various voltages is presented and confronted with actual, observed beam damage on crystals, which burst at the analysis spot. Finally, theoretical energy dispersive spectroscopy spectra for all the ettringite group minerals have been computed as well as Monte Carlo modelling of the electron-matter interaction zone. The knowledge of the estimation of the size of this zone may thus be helpful for the understanding of energy dispersive spectroscopy analysis in cement pastes or ettringite-remediated soils.

Introduction

Ettringite, also known as calcium sulphoaluminate, is the most important solid phase of the AFt group, where AFt stands for alumina, ferric oxide, tri-sulphate (or Al_2O_3 - Fe_2O_3 - tri), also denoted $[Ca_3(Al,Fe)(OH)_6{\cdot}12\ H_2O]_2{\cdot}X_3{\cdot}nH_2O$ where X represents a doubly charged anion (e.g. SO_4^{2-} for ettringite) or, sometimes, two singly charged anions. In Portland cement, ettringite is one of the first phases to form during hydration (Mehta & Monteiro, 1993). It is also a major phase formed during the hydration of calcium sulphoaluminate cements (Glasser & Zhang, 2001; Gastaldi *et al.*, 2009; Winnefeld & Lothenbach, 2010). The solid solution between end-members of the ettringite group has thus attracted interest in cementitious materials (Poellmann *et al.*, 1993, 1990; Barnett *et al.*, 2002; Macphee & Barnett, 2004; Möschner *et al.*, 2009; Leisinger *et al.*, 2010).

Ettringite also plays an important role in sulphate removal from water (Tait *et al.*, 2009), in dental cements (Camilleri, 2008), in polluted soils treatment (Ouhadi & Yong, 2008) and more generally as a phase for waste ions immobilization (Gougar *et al.*, 1996).

However, ettringite, $Ca_6Al_2(SO_4)_3(OH)_{12}.26H_2O$, or $C_6A\bar{S}_3H_{32}$, also belongs to a wider mineral group, the ettringite group minerals (EGMs), consisting of 13 end-members (Table 1). As a rare mineral (Fig. 1) formed in specific geological environments (Hurlbut & Baum, 1960; Stoppa *et al.*, 2012; Jiménez & Prieto, 2015), it was discovered at the end of the 19th century in the Eifel region, Germany; its name recalls its type locality, Ettringen (Lehmann, 1874).

Scanning electron microscopy (SEM) coupled with energy dispersive spectroscopy (EDS) for microanalysis is nowadays routinely used in cement and concrete research (Scrivener, 2004; Stutzman, 2004). Based on electron-matter interactions (Reimer, 1998), it allows high magnification imaging of fractures as well as Z-contrast (Lloyd, 1987) between phases of different density.

EDS is a fast way to gain local semiquantitative to quantitative (Newbury & Ritchie, 2015) chemical analysis and chemical mapping as well as linescans of minerals and materials. However, as outlined by Wong & Buenfeld (2006), the interaction volume resulting from the incident electron beam can be significantly larger than the probe size. More specifically, in

Correspondence to: Vincent Thiery, IMT Lille-Douai, Institut Mines Télécom, Department of Civil & Environmental Engineering, LGCgE, F-59508 Douai, France. Tel: 00 33 (0)3 27 71 24 28; fax: 00 33 (0)3 27 71 29 16; e-mail: vincent.thiery@imt-lille-douai.fr

Table 1. The ettringite group minerals (EGM).

Name	Structural formula	Density	Reference
Bentorite	$Ca_6(Cr^{3+},Al)_2(SO_4)_3(OH)_{12} \cdot 26H_2O$	2.021 (meas.)	(Gross, 1980)
Buryatite	$Ca_3(Si,Fe,Al)(SO_4)[B(OH)_4]O(OH)_5 \cdot 12H_2O$	1.895 (calc.)	(Malinko *et al.*, 2001)
Carraraite	$Ca_3(SO_4)[Ge(OH)_6](CO_3) \cdot 12H_2O$	1.979 (calc.)	(Merlino & Orlandi, 2001)
Charlesite	$Ca_6(Al,Si)_2(SO_4)_2[B(OH)_4](OH,O)_{12} \cdot 26H_2O$	1,77 (meas.)	(Dunn *et al.*, 1983)
Ettringite	$Ca_6Al_2(SO_4)_3(OH)_{12} \cdot 26H_2O$	1.77 (meas.)	(Bannister *et al.*, 1936)
Hielscherite	$Ca_3Si(SO_4)(SO_3)(OH)_6 \cdot 11H_2O$	1,82 (meas.)	(Pekov *et al.*, 2012)
Imayoshiite	$Ca_3Al(CO_3)[B(OH)_4](OH)_6 \cdot 12H_2O$	1,79 (calc.)	(Nishio-Hamane *et al.*, 2015)
Jouravskite	$Ca_3Mn^{4+}(SO_4)(CO_3)(OH)_6 \cdot 12H_2O$	1.95 (meas.)	(Gaudefroy & Permingeat, 1965)
Kottenheimite	$Ca_3Si(SO_4)_2(OH)_6 \cdot 12H_2O$	1.92 (meas.)	(Chukanov *et al.*, 2012)
Micheelsenite	$(Ca,Y)_3Al(HPO_4,CO_3)(CO_3)(OH)_6 \cdot 12H_2O$	2.83 (meas.)	(McDonald *et al.*, 2001)
Sturmanite	$Ca_6(Fe^{3+},Al,Mn^{3+})_2(SO_4)_2[B(OH)_4](OH)_{12} \cdot 25H_2O$	1.847 (meas.)	(Peacor *et al.*, 1983)
Tatarinovite	$Ca_3Al(SO_4)[B(OH)_4](OH)_6 \cdot 12H_2O$	1.79 (meas.)	(Chukanov *et al.*, 2016)
Thaumasite	$Ca_3(SO_4)[Si(OH)_6](CO_3) \cdot 12H_2O$	1.877 (meas.)	(Anthony *et al.*, n.d.)

Fig. 1. Ettringite crystals from the N'Chwaning mine, South Africa.

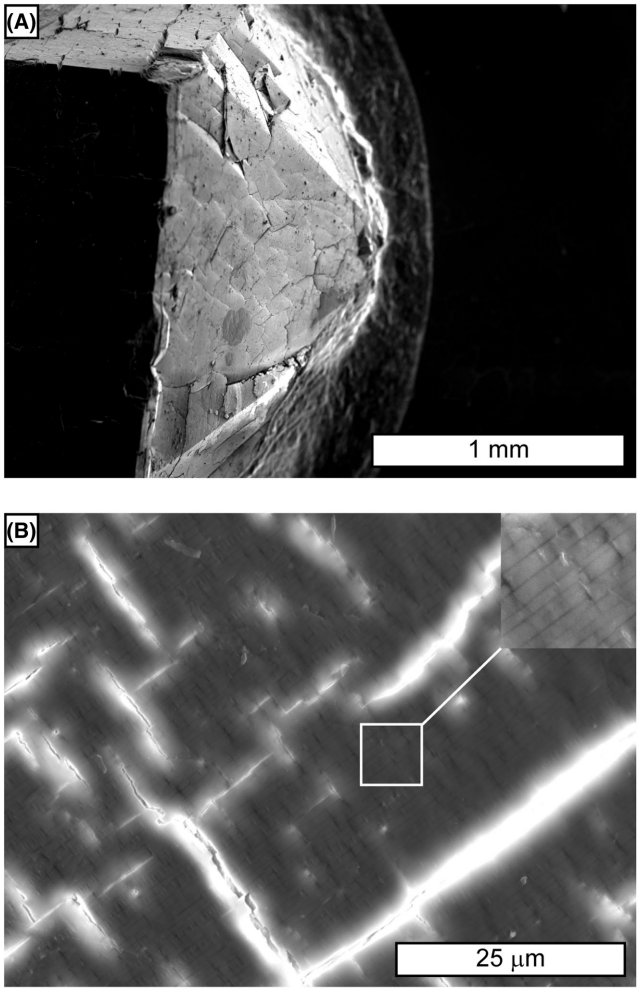

Fig. 2. (A) Termination of an ettringite crystal showing scaling due to dehydration. (B) Detail of the cracking pattern developed on crystal faces, the insert highlights the natural, regular striation of the crystal. Images acquired at 5 kV.

complex microstructures such as cement pastes where phases develop a 3D porous network from the nanometric to the micrometric range (Skibsted & Hall, 2008; Yio *et al.*, 2015), it is important to understand what volume is analysed.

EDS analysis can be simulated by Monte Carlo modelling (Gauvin, 2005), especially by using user-friendly software (Drouin *et al.*, 2007); this has yielded interesting results on cement-based materials (Wong & Buenfeld, 2006). The goal of such modelling is to gain insights of the interaction volume between the incident electrons and the sample.

The goal of the present study is to analyse natural ettringite crystals in the scanning electron microscope and to characterize the beam damage associated with microanalysis at various acceleration voltages. The purpose of such a study is (1) to complement and extend already published Monte Carlo simulations of EDS analysis on cementitious materials (Wong & Buenfeld, 2006) on the whole EGMs; (2) to discuss some limitations of EDS analysis on such minerals and (3) to confront

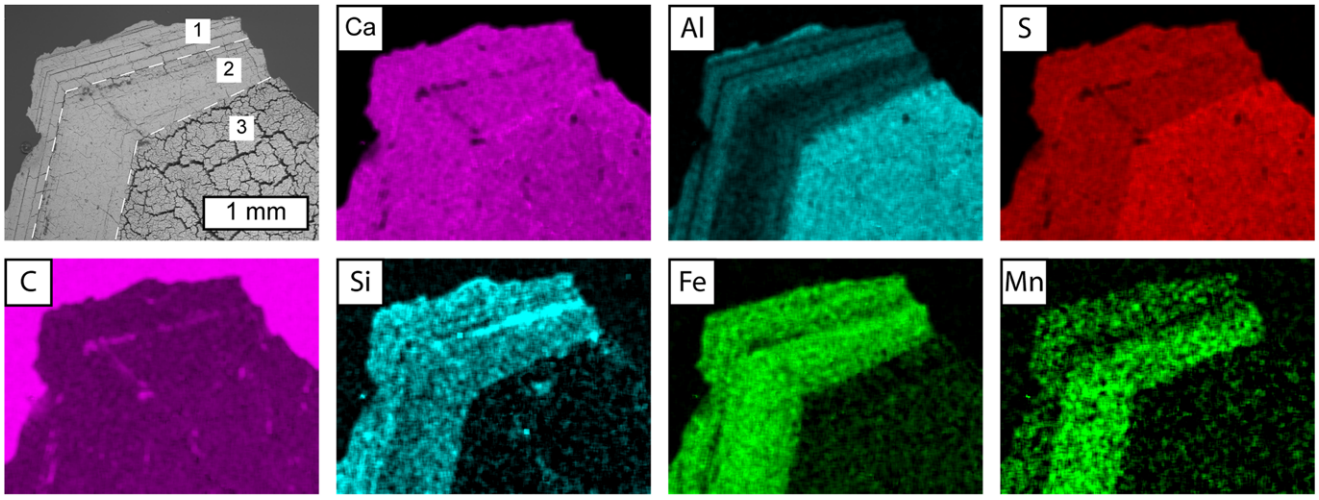

Fig. 3. EDS chemical mapping (acceleration voltage: 15kV) of an ettringite crystal embedded in resin and polished, highlighting the diversity of its chemical composition. Oxygen not shown.

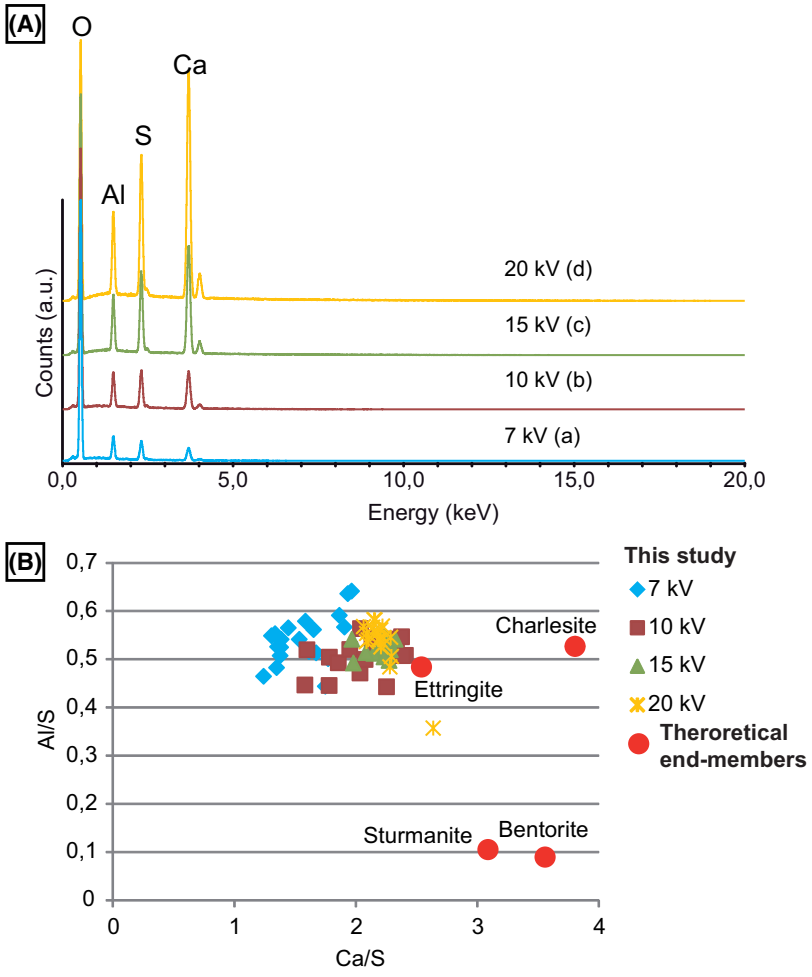

Fig. 4. (A) EDS spectra acquired at 7, 10, 15 and 20 kV on a polished section of ettringite (inner part – zone 3 – of the crystal illustrated by EDS chemical maps on Fig. 3). (B) Composition obtained using EDS analysis, presented as atomic Al/S versus Ca/S ratios and confronted with theoretical end-members compositions. See Table 1 for the references for the end-members analysis used for the calculations.

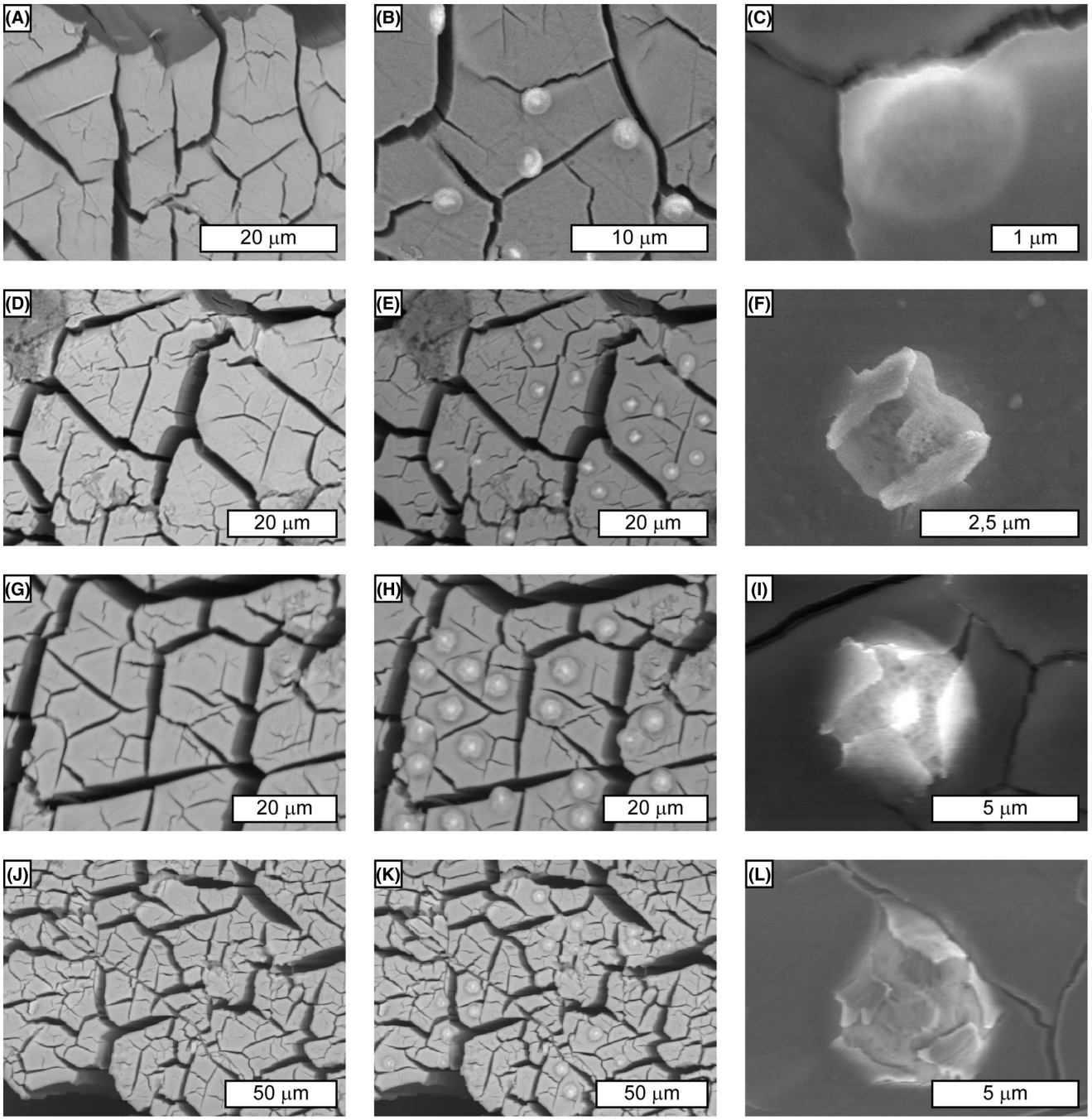

Fig. 5. Triplets of images showing an area before and after analysis and a close-up view of the resulting beam damage. (A–C): 7 kV; (D–F): 10 kV; (G–I): 15 kV; (J–L): 20 kV. Counting time 60 s.

more specifically standardless EDS analysis with accurate end-members analysis of Ca-S-Al bearing end-members of the EGM.

The EGMs

Ettringite belongs to the EGMs (Table 1) and thus solid solutions between pure end-members or intermediate compositions may occur (Carpenter, 1963; Barnett *et al.*, 2002; Macphee & Barnett, 2004; Möschner *et al.*, 2009) as well as intergrowths. For example, bentorite (Cr-ettringite) has been described in the hydration products of Cr-bearing wastes mixed with cement (Trezza & Ferraiuelo, 2003); charlesite (B-bearing ettringite) may be used to immobilize boron in radioactive wastes (Atabek *et al.*, 1992), whereas thaumasite is

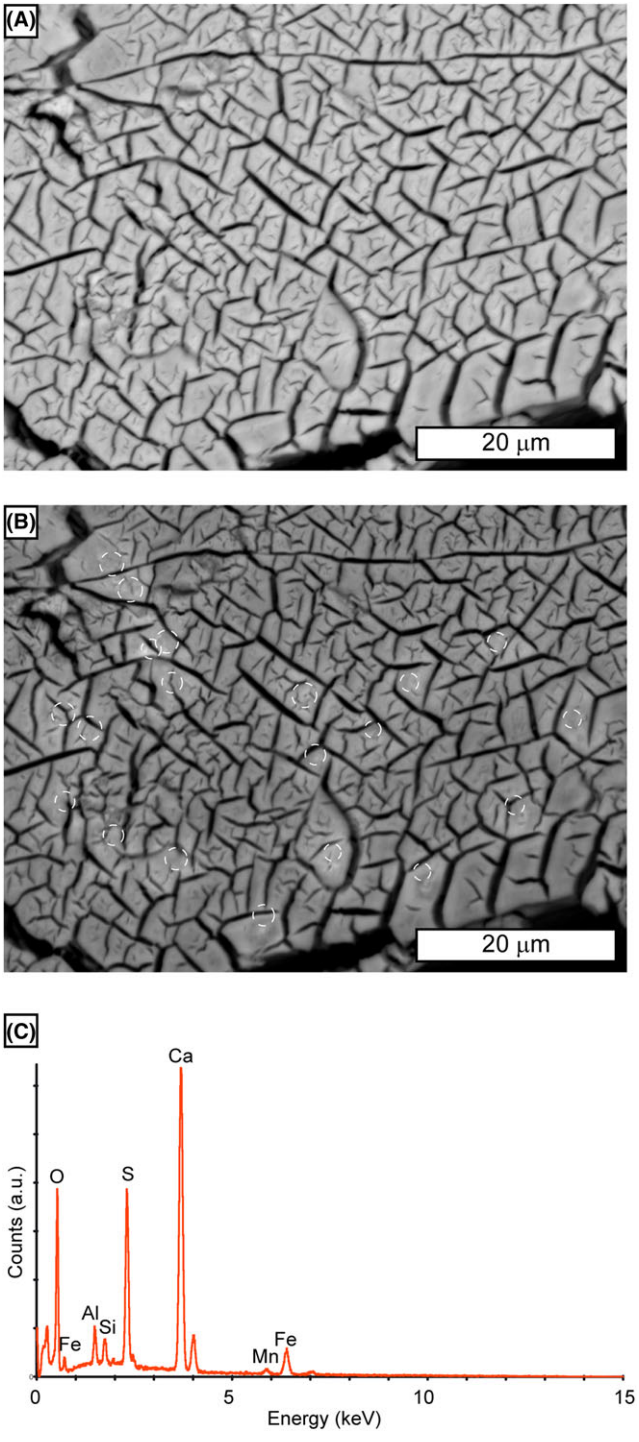

Fig. 6. (A and B) Outer part (zone 1) of the crystal illustrated by the EDS chemical maps in Figure 3 showing a better resistance to beam damage than the inner part of the crystal (analyses spots are at the centre of circles drawn in (B), a slight discolouration can be seen., (C) Representative spectrum acquired on this area.

well known in some cases of sulphate attack (Menéndez *et al.*, 2013).

Materials and methods

Natural ettringite (Fig. 1) from the N'Chwaning Mine, Kalahari manganese field, South Africa, was used in this study. Indeed, crystals from this occurrence are often used as reference natural analogues in cement research (Speziale *et al.*, 2008; Jiménez & Prieto, 2015). They may potentially be intergrown with other EGMs such as sturmanite (Pohwat, 2012) and are thus likely to widen the discussion towards other members of the EGMs. Both raw crystals and polished sections (final polishing using ¼ micrometre diamond pastes) were studied. SEM was done on a field-emission gun Hitachi S-4300SE/N SEM working in high vacuum mode, coupled to a Thermo Scientific Ultradry EDX detector. The EDS analysis was carried out standardless at 7, 10, 15 and 20 kV (the counting rate was too weak below 7 kV). The intensity was measured using a Faraday cup and was of 1.8 nA at 10kV, 3.54 nA at15 kV and 3.8 nA at 20 kV.

Monte Carlo simulations of the interaction volume of analysis were done using the CASINO software (Drouin *et al.*, 2007), and simulated EDS spectra were computed using the NIST-DTSA software (Ritchie, 2011) considering identical analytical conditions (working distance of 15 mm, no tilt of the surface).

Ettringite under the SEM: analytical results

Raw crystals

Raw crystals placed under vacuum present a phenomenon of scaling, as observed on the termination of the prisms (Fig. 2A). Along faces, a cracking pattern develops, under the form of widely opened fractures perpendicular and parallel to the elongation (Fig. 2B).

Crystal chemistry

A pluri-millimetric crystal was impregnated in epoxy resin and a cross section was done perpendicularly to its elongation axis. EDS chemical maps were acquired at 15 kV (Fig. 3). Three domains can be characterized. The innermost (number 3 on Fig. 3) is homogeneous in composition and corresponds to an area in which BSE mode reveals an intense cracking. Its chemistry (Ca, Al, S, O) corresponds to ettringite s.s., as outlined by EDS spectra (Fig. 4). An intermediate domain (number 2 on Fig. 3) of homogeneous composition is characterized by a dramatic drop in Al content and the apparition of Mn, Fe and Si. This domain shows less cracking. The outermost domain (number 1 on Fig. 3) shows regular banding with variations in Al, Ca, S and Si content as well as a lesser amount in Mn than the intermediate domain.

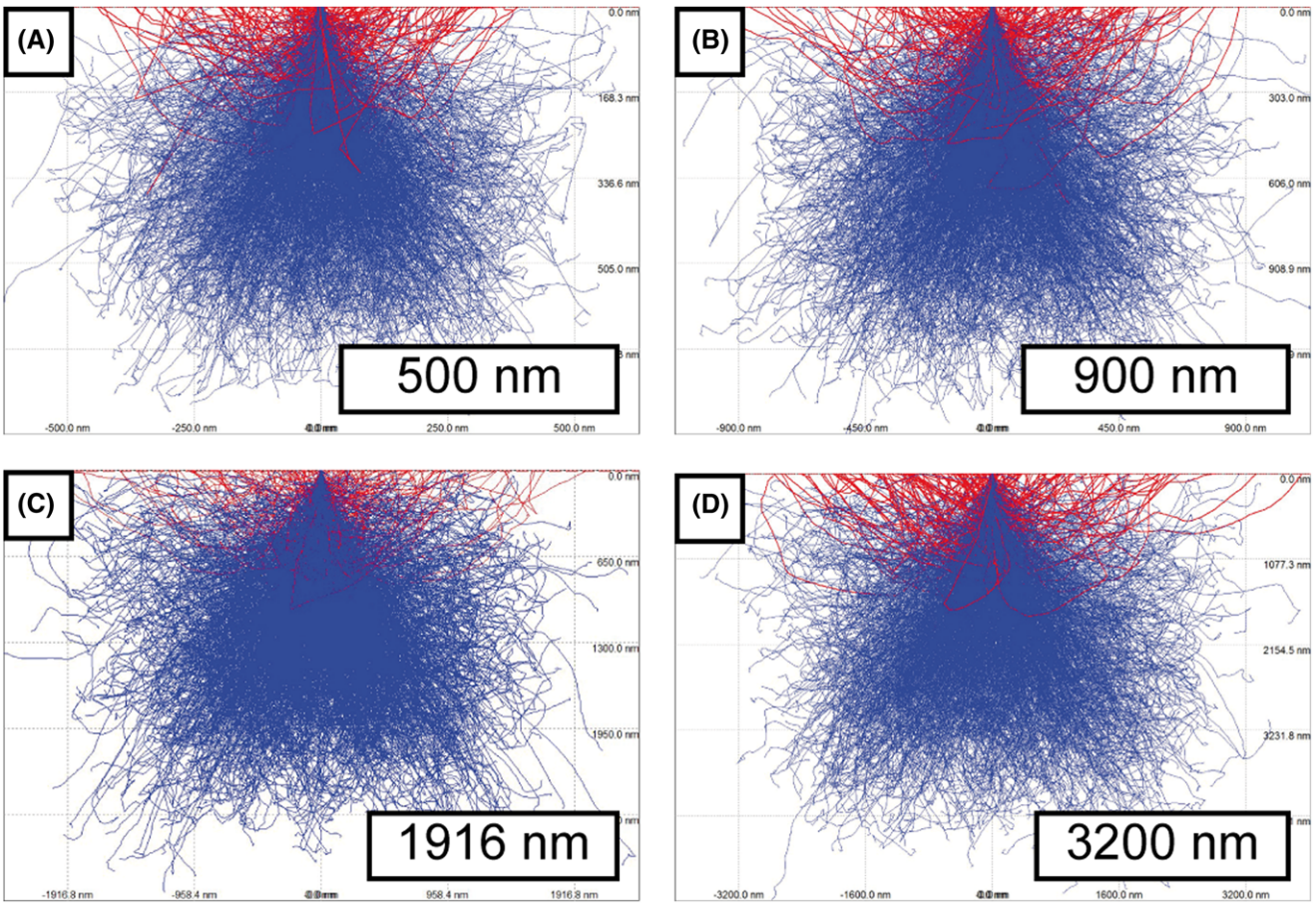

Fig. 7. Interaction volume modelled with Casino (Drouin *et al.*, 2007) for ettringite at 7 kV (A), 10 kV (B), 15 kV (C) and 20 kV (D); see Figure 4 for the corresponding spectra obtained on natural crystals.

EDS analysis and associated beam damage

The relative peak intensities of ettringite at various acceleration voltages are presented in Figure 4(A) as well as the semi-quantitative composition presented as Al/S and Ca/S ratios (Fig. 4B).

It can be seen that the relative intensities for Al, S and Ca are dependent of the accelerating voltage applied for the analysis. At the lowest voltage (7 kV), the relative peak intensities for those three peaks are opposite to what is observed at 15 and 20 kV, whereas at 10 kV the relative intensities are not intrinsically different.

Ettringite crystals, even when embedded in resin, develop a very typical dehydration cracking pattern similar to what can be observed when mud dessicates; this pattern has already been illustrated in the literature as, for example, on ettringite in sulphoaluminate cement pastes (Ambroise *et al.*, 2009; Chen *et al.*, 2012) or on natural kottenheimite (Chukanov *et al.*, 2012 and Table 1). However, as seen in Figure 3, this pattern seems to be dependent on the crystal chemistry and so is the sample damage associated with the analysis (Figs. 5 and 6). Indeed, the pattern which develops in more siliceous domains is smaller than in pure ettringite.

The interaction between the electron beam and the sample during analysis results in heating. The analysis spots (Fig. 5) are characterized by surface bursting; the size of the damaged zone is larger when the voltage increases.

However, as for the cracking pattern, this bursting seems dependent on the chemistry. Indeed, as presented in Figure 6, the more siliceous compounds (i.e. the intermediate compound between ettringite and charlesite) show a better resistance.

Monte Carlo modelling of electron–sample interaction

Ettringite s.s.

The experimental results presented up above can be approached by means of Monte Carlo modelling of electron–sample interaction.

For pure ettringite (Fig. 7), the interaction volume dramatically increases with the voltage. This is in good agreement with the bursting illustrated in Figure 5.

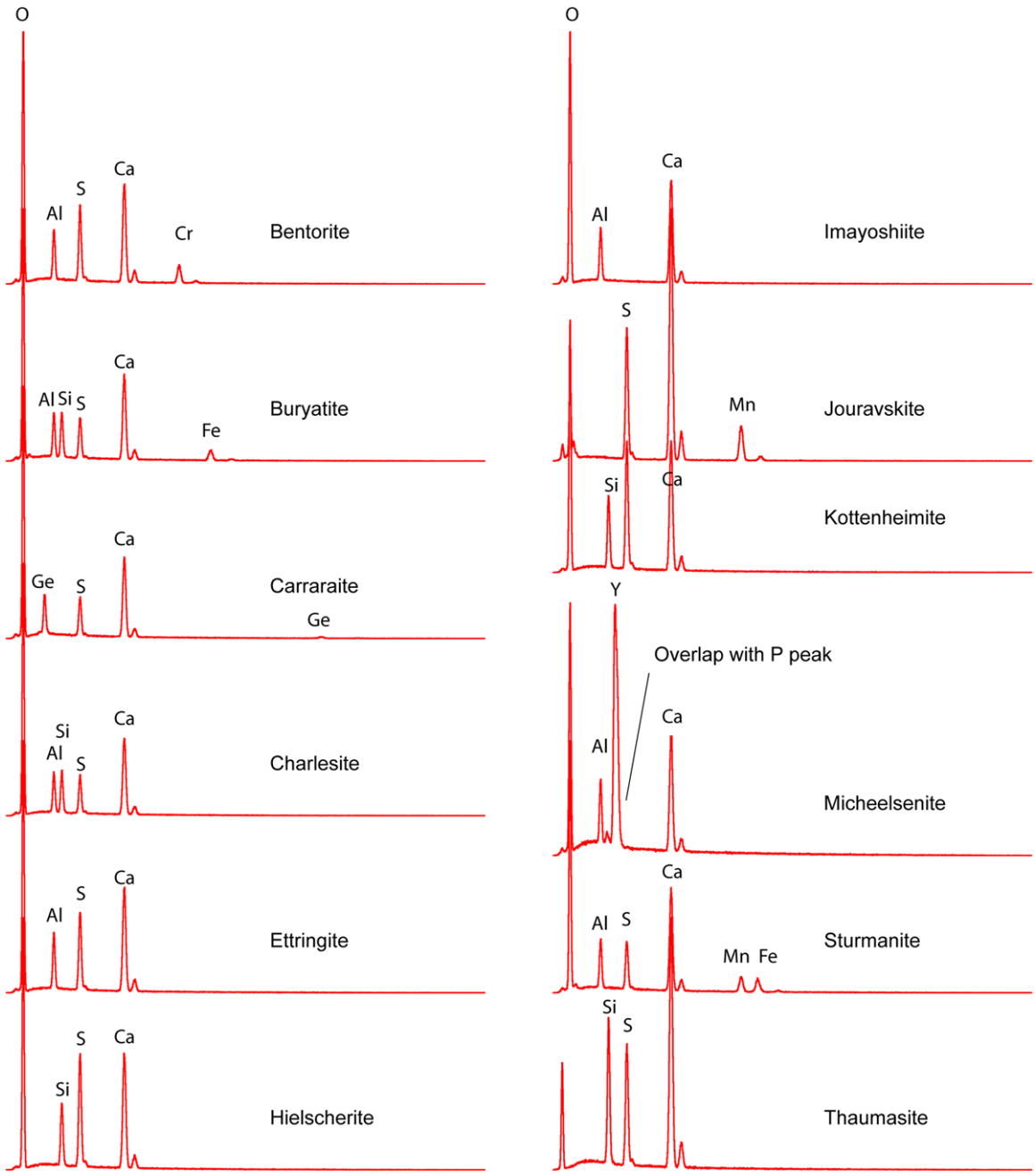

Fig. 8. Modelled EDS spectra using NIST-DTSA (Ritchie, 2011) for the ettringite group minerals at 15 kV.

The EGMss

Based on a review of the EGM, a tentative synthesis of their theoretical EDS spectra at 15 kV is presented in Figure 8, exception made for tatarinovite (Table 1) for which no density is available in the literature. In order to confront those spectra with a modelled interaction volume, Monte Carlo modelling has been carried out on all the EGM (Fig. 9) at 15 kV, which is the recommended voltage for EDS microanalysis of cementitious materials (Harrisson *et al.*, 1987).

Discussion and perspectives

It has already been proposed that among the EGM group, changes in chemical composition can explain differences in behaviour under the electron microscope due to differences in crystal structures during dehydration (Lachowski *et al.*, 2003). Ettringite is known to dehydrate and its crystal structure changes when heated (Skoblinskaya *et al.*, 1975; Skoblinskaya & Krasilnikov, 1975; Hartman *et al.*, 2006; Guimarães *et al.*, 2016).

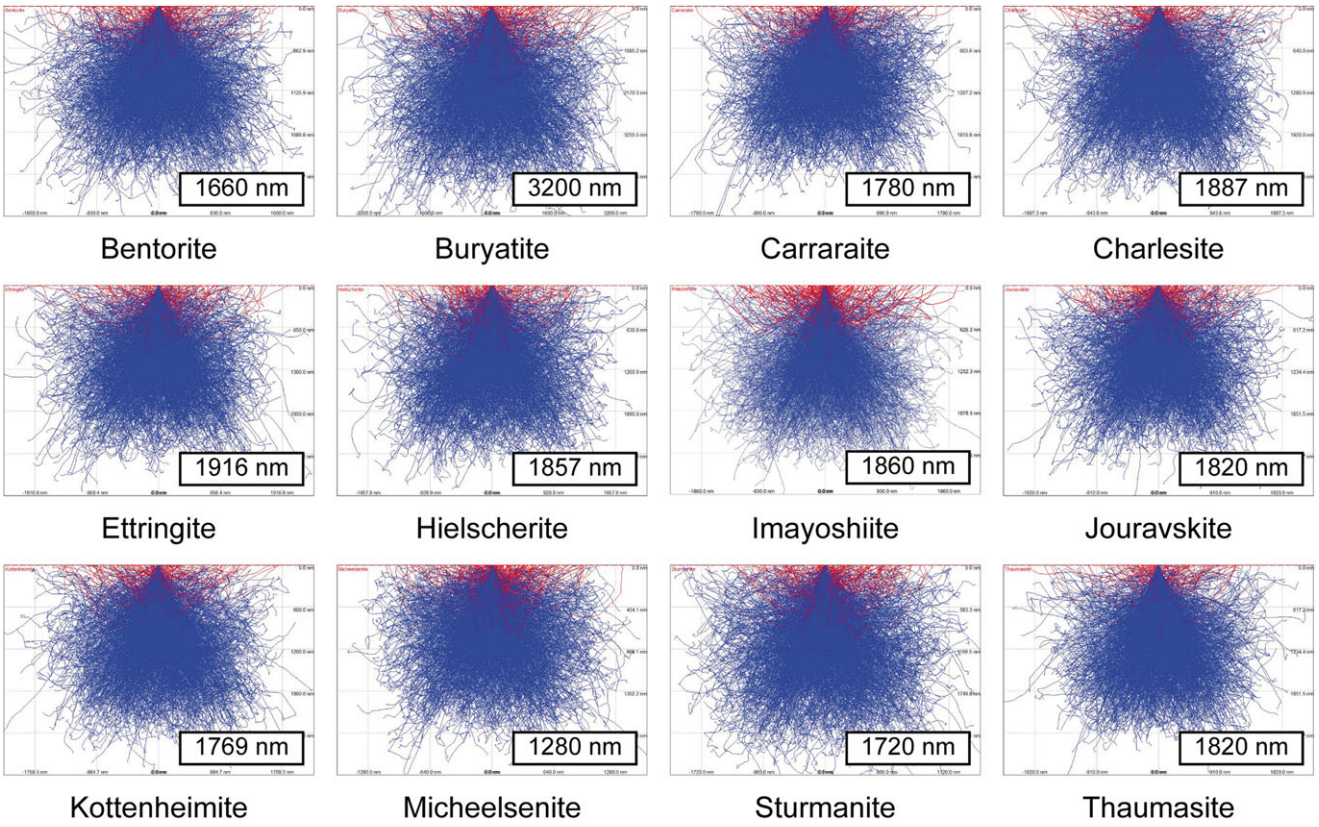

Fig. 9. Interaction volume for the ettringite group minerals at 15 kV.

SEM micrographs have shown that ettringite dehydration results in extensive cracking of crystals (Fig. 2), even on a polished section (Fig. 5), as well as bursting during analysis. Thus, the flat geometry of the sample is lost. Quantitative analysis on such distorted surfaces is difficult since the quantifications results are highly dependent on the flatness of the surface, the slightest angle being responsible for a change in the analysis (Newbury & Ritchie, 2015).

Recent advances in imaging techniques have allowed to highlight the extreme complexity and heterogeneity of the hydration products/unhydrated grains in the cement paste at micrometric scales (Trtik *et al.*, 2011; Voltolini *et al.*, 2013) and also of the porosity (Yio *et al.*, 2015). The Monte Carlo modelling of EDS analyses of the EGMs presented in this study (Fig. 9) has shown that the interaction volumes can be significantly larger than the sizes of the crystals present in a cement paste, as already shown in an earlier study (Wong & Buenfeld, 2006). Indeed, some recent studies on calcium sulphoaluminate cements have illustrated micrometric ettringite (Rungchet *et al.*, 2016) as complex intergrowths with other cementitous phases, which are thus likely to be analysed as a whole.

Moreover, the modelling results of the present study consider ettringite as a homogeneous, nonporous phase. Ettringite in cement media will coexist with a wide range of porosity, from the nanometric scale to the microscale (Jennings & Bullard, 2011): it is known that EDS analysis is greatly affected by porosity.

Finally, the chemistry of synthetic analogues of the EGM may become even more complex in a close future with the advent of sulphoaluminate cements made with various wastes (Imbabi *et al.*, 2012). SEM-EDS may be useful only for a rough estimation of the chemistry of the 'ettringite' in such environments, and a more thorough characterization may become necessary, by using, for example, thermo-gravimetry, which has proven to be efficient decipher crystal chemistry for several EGMs (Drebushchak *et al.*, 2013), as well as Raman spectroscopy (Frost *et al.*, 2013).

Acknowledgement

Christelle Van Der Merwe, Assore Ltd., is greatly acknowledged for the samples.

References

Ambroise, J., Georgin, J.F., Peysson, S. & Péra, J. (2009) Influence of polyether polyol on the hydration and engineering properties of calcium sulfoaluminate cement. *Cem. Concr. Compos.* **31**, 474–482.

Anthony, J.W., Bideaux, R.A., Bladh, K.W. & Nichols, M.C. n.d. Handbook of Mineralogy, Mineralogical Society of America, Chantilly, VA 20151-1110, USA. http://www.handbookofmineralogy.org/. [WWW Document].

Atabek, R., Bouniol, P., Vitorge, P., Le Bescop, P. & Hoorelbeke, J.M. (1992) Cement use for radioactive waste embedding and disposal purposes. *Cem. Concr. Res.* **22**, 419–429.

Bannister, F.A., Hey, M.H. & Bernal, J. (1936) Ettringite from Scawt Hill, Co. *Antrim. Mineral. Mag.* **24**, 324–329.

Barnett, S.J., Macphee, D.E., Lachowski, E.E. & Crammond, N.J. (2002) XRD, EDX and IR analysis of solid solutions between thaumasite and ettringite. *Cem. Concr. Res.* **32**, 719–730.

Camilleri, J. (2008) Characterization of hydration products of mineral trioxide aggregate. *Int. Endod. J.* **41**, 408–417.

Carpenter, A.B. (1963) Oriented overgrowths of thaumasite on ettringite. *Am. Mineral.* **48**, 1394–1396.

Chen, I.A., Hargis, C.W. & Juenger, M.C.G. (2012) Understanding expansion in calcium sulfoaluminate-belite cements. *Cem. Concr. Res.* **42**, 51–60.

Chukanov, N.V., Britvin, S.N., Van, K.V., Möckel, S. & Zadov, A.E. (2012) Kottenheimite, $Ca_3Si(OH)_6(SO_4)_2{\cdot}12H_2O$, a new member of the ettringite group from the Eifel area, Germany. *Can. Mineral.* **50**, 55–63.

Chukanov, N.V., Kasatkin, A.V., Zubkova, N.V., Britvin, S.N., Pautov, L.A., Pekov, I.V., Varlamov, D.A., Bychkova, Ya.V., Loskutov, A.B., Novgorodova, E.A. (2016) Tatarinovite $Ca_3Al(SO_4)[B(OH)_4](OH)_6{\cdot}12H_2O$ — A new ettringite-groupmineral from the bazhenovskoe deposit (the middle urals, russia), and its crystal structure zapiski rmo (proceedings of the russian mineralogical society) Pt cxlv, *N 1*. 48–67.

Drebushchak, V.A., Seryotkin, Y.V., Kokh, S.N. & Sokol, E.V. (2013) Natural specimen of triple solid solution ettringite-thaumasite-chromate-ettringite. *J. Therm. Anal. Calorim.* **114**, 777–783.

Drouin, D., Réal Couture, A., Joly, D., Tastet, X., Aimez, V. & Gauvin, R. (2007) CASINO V2.42—a fast and easy-to-use modeling tool for scanning electron microscopy and microanalysis users. *Scanning* **29**, 92–101.

Dunn, P.J., Peacor, D.R., Leavens, P.B. & Baum, J.L. (1983) Charlesite, a new mineral of the ettringite group, from Franklin, New Jersey. *Am. Mineral.* **68**, 1033–1037.

Frost, R.L., López, A., Xi, Y., Scholz, R., da Costa, G.M., Lima, R.M.F. & Granja, A. (2013) The spectroscopic characterization of the sulphate mineral ettringite from Kuruman manganese deposits, South Africa. *Vib. Spectrosc.* **68**, 266–271.

Gastaldi, D., Canonico, F. & Boccaleri, E. (2009) Ettringite and calcium sulfoaluminate cement: investigation of water content by near-infrared spectroscopy. *J. Mater. Sci.* **44**, 5788–5794.

Gaudefroy, C. & Permingeat, F. (1965) La jouravskite, une nouvelle espèce minérale. *Bull. la Société Française Minéralogie* **88**, 254–262.

Gauvin, R. (2005) X-ray microanalysis of real materials using Monte Carlo simulations. *Surface and Interface Analysis*. pp. 875–886. https://doi.org/10.1002/sia.2105

Glasser, F.P. & Zhang, L. (2001) High-performance cement matrices based on calcium sulfoaluminate-belite compositions. *Cem. Concr. Res.* **31**, 1881–1886.

Gougar, M.L.D., Scheetz, B.E. & Roy, D.M. (1996) Ettringite and C-S-H portland cement phases for waste ion immobilization: a review. *Waste Manag.* **16**, 295–303.

Gross, S. (1980) Bentorite. A new mineral from the Hatrurim area, west of the Dead Sea, Israel. *Isr. J. Earth Sci.* **29**, 81–84.

Guimarães, D., de A. Oliveira, V. & Leão, V.A. (2016) Kinetic and thermal decomposition of ettringite synthesized from aqueous solutions. *J. Therm. Anal. Calorim.* **124**, 1679–1689.

Harrisson, A.M., Winter, N.B. & Taylor, H.F.W. (1987) X-ray microanalysis of microporous materials. *J. Mater. Sci. Lett.* **6**, 1339–1340.

Hartman, M.R., Brady, S.K., Berliner, R. & Conradi, M.S. (2006) The evolution of structural changes in ettringite during thermal decomposition. *J. Solid State Chem.* **179**, 1259–1272.

Hurlbut, C.S. & Baum, J.L. (1960) Ettringite from Franklin, New Jersey. *Am. Mineral.* **45**, 1137–43.

Imbabi, M.S., Carrigan, C. & McKenna, S. (2012) Trends and developments in green cement and concrete technology. *Int. J. Sustain. Built Environ.* **1**, 194–216.

Jennings, H.M. & Bullard, J.W. (2011) From electrons to infrastructure: engineering concrete from the bottom up. *Cem. Concr. Res.* **41**, 727–735.

Jiménez, A. & Prieto, M. (2015) Thermal stability of ettringite exposed to atmosphere: implications for the uptake of harmful ions by cement. *Environ. Sci. Technol.* **49**, 7957–7964.

Lachowski, E.E., Barnett, S.J. & Macphee, D.E. (2003) Transmission electron optical study of ettringite and thaumasite. *Cement and Concrete Composites*. **25**, 819–822.

Lehmann, J. (1874) Über den ettringit, ein neues mineral, in Kalkeinschlüssen der Lava von Ettringen (Laacher Gebiet). *Neues Jahrb. für Mineral. Geol. und Palaontologie* 273–275.

Leisinger, S.M., Lothenbach, B., Le Saout, G., Kägi, R., Wehrli, B. & Johnson, C.A. (2010) Solid solutions between CrO4- and SO4-ettringite Ca6(Al(OH)6)2[(CrO4)x(SO4)(1-x)]3*26 H2O. *Environ. Sci. Technol.* **44**, 8983–8988.

Lloyd, G.E. (1987) Atomic number and crystallographic contrast images with the SEM: a review of backscattered electron techniques. *Mineral. Mag.* **51**, 3–19.

Macphee, D.E. & Barnett, S.J. (2004) Solution properties of solids in the ettringite—thaumasite solid solution series. *Cem. Concr. Res.* **34**, 1591–1598.

Malinko, S.V., Chukanov, N.V., Dubinchuk, V.T., Zadov, A.E. & Koporulina, E.V. (2001) Buryatite Ca3(Si, Fe3+, Al)[SO4][B(OH)4](OH)5O·12H2O, a new mineral. *Zap. Vseross. Mineral. Obs.* **130**, 72–78.

McDonald, A.M., Peterson, O. V., Gault, R.A., Johnsen, O., Niedermayr, G., Brandstätter, F. & Giester, G. (2001) Micheelsenite, (Ca,Y)3Al(PO3OH,CO3)(CO3)(OH)6·12H2O, a new mineral from Mont Saint–Hilaire, Quebec, Canada and the Nanna pegmatite, Narsaarsuup Qaava, South Greenland. *Neues Jahrb. Fur Mineral.* Monatshefte: **8**, 337–351.

Mehta, P.K. & Monteiro, P.J.M. (1993) *Concrete. Structure, Properties, and Materials*. Prentice Hall. Upper Saddle River, 450 p.

Menéndez, E., Matschei, T. & Glasser, F. (2013) Sulfate attack of concrete. *Performance of Cement-Based Materials in Aggressive Aqueous Environments* (ed. by M. Alexander, A. Bertron & N. De Belie), pp. 7–74. Springer, Netherlands.

Merlino, S. & Orlandi, P. (2001) Carraraite and zaccagnaite, two new minerals from the Carrara marble quarries: their chemical compositions, physical properties, and structural features. *Am. Mineral.* **86**, 1293–1301.

Möschner, G., Lothenbach, B., Winnefeld, F., Ulrich, A., Figi, R. & Kretzschmar, R. (2009) Solid solution between Al-ettringite and Fe-ettringite (Ca6[Al1−xFex(OH)6]2(SO4)3·26H2O). *Cem. Concr. Res.* **39**, 482–489.

Newbury, D.E. & Ritchie, D.W.M. (2015) Performing elemental microanalysis with high accuracy and high precision by scanning electron microscopy/silicon drift detector energy-dispersive X-ray spectrometry (SEM/SDD-EDS). *J. Mater. Sci.* **50**, 493–518.

Nishio-Hamane, D., Ohnishi, M., Momma, K., Shimobayashi, N., Miyawaki, R., Minakawa, T. & Inaba, S. (2015) Imayoshiite, Ca3Al(CO3)[B(OH)4](OH)6·12H2O, a new mineral of the ettringite group from Ise City, Mie Prefecture, Japan. *Mineral. Mag.* **79**, 413–423.

Ouhadi, V.R. & Yong, R.N. (2008) Ettringite formation and behaviour in clayey soils. *Appl. Clay Sci.* **42**, 258–265.

Peacor, D.R., Dunn, P.J. & Duggan, M. (1983) Sturmanite, a ferric iron, boron analogue of ettringite. *Can. Mineral.* **21**, 705–709.

Pekov, I.V, Chukanov, N.V, Britvin, S.N., *et al.* (2012) The sulfite anion in ettringite-group minerals: a new mineral species hielscherite, Ca3Si(OH)6(SO4)(SO3)·11H2O, and the thaumasite-hielscherite solid-solution series. *Mineral. Mag.* **76**, 1133–1152.

Poellmann, H., Auer, S., Kuzel, H.-J. & Wenda, R. (1993) Solid solution of ettringites part II: incorporation of B(OH)4- and CrO42- in 3CaO.Al2O3.3CaSo4.32H2O. *Cem. Concr. Res.* **23**, 422–430.

Poellmann, H., Kuzel, H.J. & Wenda, R. (1990) Solid solution of ettringites part I: incorporation of OH- and CO32- in 3CaO.A12O3.32H2O. *Cem. Concr. Res.* **20**, 941–947.

Pohwat, P.W. (2012) Ettringite, N'Chwaning II Mine, Northern Cape Province, Republic of South Africa. *Rocks Miner.* **87**, 430–435.

Reimer, L. (1998) *Scanning Electron Microscopy Physics of Image Formation and Microanalysis*. Springer, Berlin-Heidelberg.

Ritchie, N. (2011) Getting started with NIST* DTSA-II. *Micros. Today* **19**, 26–31.

Rungchet, A., Chindaprasirt, P., Wansom, S. & Pimraksa, K. (2016) Hydrothermal synthesis of calcium sulfoaluminate–belite cement from industrial waste materials. *J. Clean. Prod.* **115**, 273–283.

Scrivener, K.L. (2004) Backscattered electron imaging of cementitious microstructures: understanding and quantification. *Cem. Concr. Compos.* **26**, 935–945.

Skibsted, J. & Hall, C. (2008) Characterization of cement minerals, cements and their reaction products at the atomic and nano scale. *Cem. Concr. Res.* **38**, 205–225.

Skoblinskaya, N.N. & Krasilnikov, K.G. (1975) Changes in crystal structure of ettringite on dehydration. 1. *Cem. Concr. Res.* **5**, 381–393.

Skoblinskaya, N.N., Krasilnikov, K.G., Nikitina, L.V. & Varlamov, V.P. (1975) Changes in crystal structure of ettringite on dehydration. 2. *Cem. Concr. Res.* **5**, 419–431.

Speziale, S., Jiang, F., Mao, Z., Monteiro, P.J.M., Wenk, H.-R., Duffy, T.S. & Schilling, F.R. (2008) Single-crystal elastic constants of natural ettringite. *Cem. Concr. Res.* **38**, 885–889.

Stoppa, F., Scordari, F., Mesto, E., Sharygin, V.V & Bortolozzi, G. (2012) Calcium-aluminum-silicate-hydrate "cement" phases and rare Ca-zeolite association at Colle Fabbri, Central Italy. *Cent. Eur. J. Geosci.* **2**, 175–187.

Stutzman, P. (2004) Scanning electron microscopy imaging of hydraulic cement microstructure. *Cem. Concr. Compos.* **26**, 957–966.

Tait, S., Clarke, W.P., Keller, J. & Batstone, D.J. (2009) Removal of sulfate from high-strength wastewater by crystallisation. *Water Res.* **43**, 762–772.

Trezza, M.A. & Ferraiuelo, M.F. (2003) Hydration study of limestone blended cement in the presence of hazardous wastes containing Cr(VI). *Cem. Concr. Res.* **33**, 1039–1045.

Trtik, P., Münch, B., Gasser, P., Leemann, A., Loser, R., Wepf, R. & Lura, P. (2011) Focussed ion beam nanotomography reveals the 3D morphology of different solid phases in hardened cement pastes. *J. Microsc.* **241**, 234–242.

Voltolini, M., Dalconi, M.C., Artioli, G., Parisatto, M., Valentini, L., Russo, V., Bonnin, A. & Tucoulou, R. (2013) Understanding cement hydration at the microscale: new opportunities from "pencil-beam" synchrotron X-ray diffraction tomography. *J. Appl. Crystallogr.* **46**, 142–152.

Winnefeld, F. & Lothenbach, B. (2010) Hydration of calcium sulfoaluminate cements — experimental findings and thermodynamic modelling. *Cem. Concr. Res.* **40**, 1239–1247.

Wong, H.S. & Buenfeld, N.R. (2006) Monte Carlo simulation of electron-solid interactions in cement-based materials. *Cem. Concr. Res.* **36**, 1076–1082.

Yio, M.H.N., Mac, M.J., Wong, H.S. & Buenfeld, N.R. (2015) 3D imaging of cement-based materials at submicron resolution by combining laser scanning confocal microscopy with serial sectioning. *J. Microsc.* **258**, 151–169.